International Journal of Pharmaceutics: X 8 (2024) 100279

Contents lists available at ScienceDirect

International Journal of Pharmaceutics: X

journal homepage: www.sciencedirect.com/journal/international-journal-of-pharmaceutics-x

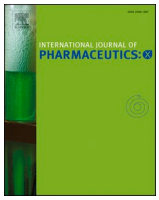

HSPiP and QbD oriented optimized stearylamine-elastic liposomes for topical delivery of ketoconazole to treat deep seated fungal infections: In vitro and ex vivo evaluations

Afzal Hussain *, Mohammad A. Altamimi *, Yaser Saleh Alneef

Department of Pharmaceutics, College of Pharmacy, King Saud University, Riyadh 11451, Saudi Arabia

A R T I C L E I N F O

Keywords:
Ketoconazole
HSPiP
Stearylamine
Cationic OKEL1
In-vitro-ex-vivo studies

A B S T R A C T

The study explored stearylamine containing cationic elastic liposomes to improve topical delivery and efficacy of ketoconazole (KETO) to treat deeply seated fungal infections. Stearylamine was used for dual functionalities (electrostatic interaction and flexibility in lipid bilayer). Hansen solubility program (HSPiP) estimated Hansen solubility parameters (HSP) based on the SMILE file and structural properties followed by experimental solubility study to validate the predicted values. Various formulations were developed by varying phosphatidylcholine and surfactants (tween 80 and span 80) concentration. To impart cationic properties, stearylamine (1.0 %) was added into the organic phase. Using quality by design (QbD) method, we optimized the formulations and evaluated for vesicle size, polydispersity index, zeta potential, morphology (scanning electron microscopy), in vitro drug release (%), and ex vivo permeation profiles. Result showed that there is a good correlation (0.65) between HSPiP predicted and actual experimental solubility of KETO in water, chloroform, S80, and tween 80. Spherical OKEL1 showed an established correlation between the predicted and the actual formulation parameters (size, zeta potential, and polydispersity index) (259 nm vs 270 nm, +2.4 vs 0.21 mV, and 0.24 vs 0.27). OKEL1 was associated with the highest value of %EE (83.1 %) as compared to liposomes. Finally, OKEL1 exhibited the highest % cumulative permeation (49.9 %) as compared to DS (13 %) and liposomes (25 %). Moreover, OKEL1 resulted in 4-fold increase in permeation flux as compared to DS which may be attributed to vesicular mediated improved permeation and gel based compensated trans epidermal water loss in the skin. The drug deposition elicited OKEL1 and OKEL1-gel as suitable carriers for maximum therapeutic benefit to treat deeply seated fungal infections.

1. Introduction

Ketoconazole (KETO) is a first-line azole antifungal agent to treat local (superficial) and systemic mycosis (deep seated fungal infection caused by *candida*, dermatophytosis, and *tinea versicolor*) (Smith and Henry, 1984). Various topical drug delivery strategies (nanoemulsion, liposomes, elastic liposomes, solid lipid nanoparticles (SLNs), and nanostructured lipid carriers as NLCs, have certain limitations (short storage stability, drug leakage from conventional liposomal lipid bilayer, and limited drug loading in SLNs, and toxic potential of polymeric NPs due to retained organic solvent) and failed to reach clinical bed. The cost of cholesterol-based liposomes, challenges in scaling up nanoemulsion production for large-scale use, and the frequent development of drug-resistant strains have restricted the clinical applications of ketoconazole in controlling fungal infections. However, researchers have made progress in enhancing its efficacy and safety (Ramzan et al., 2021). In our previous report, we explored the impact of cationic nanoemulsion to control fungal infection and the ex vivo results were found to be significantly better as compared to the control suspension (Shahid et al., 2022). Few authors reported nano-elastic liposomes loaded ketoconazole and sodium stibogluconate to treat cutaneous leishmaniosis (Dar et al., 2020). High oral dose, short elimination half-life, low molecular weight, poor aqueous solubility, and potential hepatic enzyme inhibitor related properties of the drug envisaged to formulate a cost effective and cholesterol free ketoconazole elastic liposome for topical and dermal delivery. Application of stearylamine (SA) as cationic charge inducer over others can rationalized based on various aspects associated with it. SA is biocompatible lipid in nature

* Corresponding authors.
E-mail addresses: amohammed2@ksu.edu.sa (A. Hussain), maltamimi@ksu.edu.sa (M.A. Altamimi).

https://doi.org/10.1016/j.ijpx.2024.100279
Received 6 June 2024; Received in revised form 18 August 2024; Accepted 24 August 2024
Available online 26 August 2024

with better lodging property in the lipid bilayer. It renders cationic charge for augmented electrostatic interaction between the negatively charged skin surface/fungal strain and cationic vesicles of elastic liposomes (Tahara et al., 2018). Moreover, cholesterol free elastic liposomes are responsible to produce ultra-deformable vesicles and cost effective product. Considering stearylamine in the vesicle, it was a great effort to add cationic charge and the strategy was expected to execute multiple functionalities such as improved interaction between the negatively charged skin surface and cationic vesicle for enhanced permeation, augmented internalization with negatively charged fungal hyphae, and prolonged physical stability as compared to conventional liposomes. Moreover, unique nature of biocompatible SA such as hydrophobicity, low molecular weight (~ 270 g/mol), and high pKa 10.2, is suitable for ease in lodging within phospholipid bilayer of vesicles at neutral pH (Vassoudevane et al., 2023). Notably, SA provides relatively smaller vesicles as compared to other charge inducers and it possessed innate anti-parasitic properties as liposomes [6]. Selection of SA over others was based on the safety consideration as explored in various reports using erythrocytes wherein limited hemolysis (~ 8 %) was observed (Yoshihara, et al., 1986).

Considering several benefits associated with elastic liposomes and SA, an attempt has been made to tailor KETO loaded stearylamine based liposomes using HSPiP (predictive) and QbD (optimization). In brief, HSPiP has been well explored in our laboratory to screen suitable excipients for formulation development based on Hansen parameters. HSPiP is basically operating on material energies (cohesive energy distributed over polarity energy, δ_p dispersion energy δ_d, and hydrogen bond energy δ_h) (Yoshihara, et al., 1986; Hansen, 2007). Moreover, QbD identifies various quality critical attributes (materials and process) to optimize a product with high desirability and reproducibility. The attempt has not been explored so far for SA containing elastic liposomes. Therefore, various formulations were prepared and optimized. The optimized product (OKEL1) and its gel (OKEL1-gel) were studied for comparative assessment against the drug solution (DS) and liposomes. Finally, ex vivo permeation study corroborated the relative impact of SA based elastic liposomes over conventional liposomes. The studied nanocarrier is cost-effective and scalable for the large scale production.

2. Materials and methods

2.1. Materials

Ketoconazole (KETO) is chemically (±)-cis − 1-Acetyl-4-(4-[(2-[2,4-dichlorophenyl]-2-[1H-imidazol-1-ylmethyl]-1,3-dioxolan-4-yl)-methoxy]phenyl)piperazine. KETO (CAS 65277–42-1, purity 99.0 %) and stearylamine (1-aminooctadecane, octadecylamine, purity ≥99.0 %) were procured from Sigma-Aldrich, Mumbai, India. Sodium cholate (≥ 98.5 % purity in assay) was procured from CDH Fine Chemicals, Mumbai, India. Soy phosphatidylcholine (PC), tween 80, and span 80 were procured from Spectrum Chemicals MFG Corp., New Brunswick, NJ, USA. Methanol (analytical grade) and chloroform were procured from CDH Fine Chemical, Mumbai, India. Distilled water was used as an aqueous system wherever used in the study. HSPiP (version 5.0.04, Louisville, KY, USA) was a purchased version (USA).

3. Methods

3.1. HSPiP software based predicted HSP values for excipients and the drug

HSPiP applications have been explored in analytical chemistry, paint industry, drug delivery, and rheological science. At preliminary stage of research development, the program is quite useful for rapid and cost effective solubility study to screen suitable solvent. Hansen solubility parameters (HSP) of HSPiP dictate the selection of solvent and assigned as “good” or “bad” based on relative energy difference (RED) value. Various input parameters are used to run the program to get RED (Ra/Ro) value, HSP distance, and molecular volume (mVol) as output values (Yoshihara, et al., 1986; Hansen, 2007). Mathematically, the total cohesive energy (δ_t) is expressed as eq. (1):

$$[\delta_t]^2 = [\delta_d]^2 + [\delta_p]^2 + [\delta_h]^2 \quad (1)$$

where δ_d, δ_p, and δ_H are the dispersion energy, the polarity, and the hydrogen bonding energy, respectively (Yoshihara, et al., 1986). Solvent is flagged depending upon the experimental solubility and the obtained difference of HSP parameters between the solute and the solvent (δ_{ds} - $\delta_{dv} \approx$ low, δ_{ps} - $\delta_{pv} \approx$ low, and δ_{hs} - $\delta_h \approx$ low or $\Delta(\delta_{ps}\text{-}\delta_{pv}) = 0$, $\Delta(\delta_{ds}\text{-}\delta_{dv} = 0$, and $\Delta(\delta_{hs}\text{-}\delta_{hv} = 0]$ (Yoshihara, et al., 1986). KETO is an aromatic lipophilic antifungal agent with multiple interactive forces (functional group based interactions such as π-π interactions, hydrophobic interaction, polar and nonpolar) (Abbott, 2010). Decision was made based on the combined results of HSP outcomes and the obtained experimental solubility investigated at particular temperature. Biasness was avoided while processing the input data in the program.

3.2. Analytical methodology

For the sample analysis, UV vis spectrophotometer was used. Briefly, a stock solution was freshly prepared in methanol (1 mg/mL). A serial dilution was conducted to prepare various solutions of known concentration. Methanol was used as a blank while analysis. A working calibration curve was established (1.0–100.0 μg/mL) to obtained a linear regression ($r^2 = 0.999$) for the system suitability. The drug was assayed at λ_{max} value of 254 nm. The study was replicated to get mean value and standard deviation ($n = 3$).

3.3. Differential scanning calorimeter (DSC)

It was mandatory to investigate the purity and possible contamination of the drug by thermal analysis using DSC (DSC-4000, Perkin Elmer, USA). The technique also helped to estimate the thermal parameters of KETO and crystallization behavior (Basu et al., 2018). The sample was weighed (4 mg), crimped (into aluminium pan), and placed inside the furnace. Heating rate (10 °C/min) was applied to the targeted temperature of 340 °C followed by subsequent cooling before the next sample. A cooling nitrogen chiller was used to control the cooling step. Nitrogen gas (N_2) was set at the flow rate of 20 mL/min.

3.4. Experimental solubility of KETO in the predicted solvents

The predicted excipients were selected for the real solubility in the explored excipients (chloroform, methanol, water, ethanol, PC, span 80, and tween 80) based on HSPiP. A mole fraction solubility “x^e” of KETO was carried out at $T = 318.2$ °C and fixed pressure (0.1 MPa). The drug was added into a glass vial containing the predicted excipient (2 mL). The mixture was placed inside water bath shaker previously set at constant temperature and shaking rate (100 rpm) (Hussain et al., 2021). The shaker was allowed to run for complete drug solubilization and saturation (72 h). At attained equilibrium, KETO content (μg g^{-1}) was assayed in each excipient ($n = 3$) using a UV vis spectrophotometer (U-1800, Japan). Mole fraction solubility (x^e) of KETO can be calculated using eq. (2).

$$x^e = \frac{\frac{m_1}{M_1}}{\frac{m_1}{M_1} + \frac{m_2}{M_2}} \quad (2)$$

wherein “m_1” and “M_1” are the mass (weight) and the molar mass of KETO, respectively. Similarly, m_2 and M_2 are the mass (weight) and the molar mass of the investigated solvent, respectively. Experiment was repeated for mean value.

3.5. Preparation of various trial formulations

Various formulations were prepared by varying the concentration and types of edge activators (span 80 and tween 80). A weighed amount of PC (30–90 mg), SA (5 mg), and KETO drug (20 mg) was dissolved in chloroform (present in the round bottom flask). A lipophilic span 80 was also dissolved in the mixture whereas tween 80 (hydrophilic) was dissolved in the aqueous phase (phosphate buffer solution, PBS at pH 7.4). PBS solution served as a hydrating medium containing a fixed content of ethanol (70 mg) and tween 80. Ethanol was added to serve as plasticizer of the lipid bilayer. Notably, Span 80 (S80) content was varied from 10 to 90 mg whereas a constant amount of tween 80 (15 mg) was used in each trial formulation. A combination of span 80 and tween 80 provided stable product than standalone. For optimized formulation (OKEL1), equal ratio of span 80 and tween 80 (1:1) was used and expressed as "SM". In brief, the organic phase solution was present in the RBF (round bottom flask) and allowed to be rotated on a rotatory evaporator. It developed a thin film on the inner layer of RBF. The film was completely dried and left to remove chloroform. Any moisture or water contact was avoided. The hydrating medium was used to hydrate the film and the vesicles were generated by gentle shaking. The obtained colloidal milky elastic liposomes suspensions were stored and labelled for future use.

3.6. Characterizations of the formulations

The developed formulations were evaluated for vesicle size, zeta potential, PDI values, and % entrapment efficiency (%EE). These parameters were determined as the input parameters for the optimization of the composition and desired outcome using an experimental design tool (Design Expert). Vesicle size, zeta potential, and size distribution (PDI) were determined using a Malvern zetasizer (Nano ZS, Malvern, UK). Being milky colloidal suspension of elastic liposomes, the sample was diluted with PBS solution (100 times). For the zeta potential measurement, the sample was undiluted to determine real charge density. The experiments were replicated 10 times in auto mode of the analyzer. The drug entrapment efficiency study was conducted following the reported method (described later in the running section) (Hussain et al., 2021). The total drug content was assayed using UV Vis spectrophotometer (U-1800, Japan) (Hussain et al., 2021).

3.7. Optimization using design expert

Design-Expert 13.0.12 software was used for the optimization. A mixture design model was selected and three mixture components were used as (a) PC (phosphatidylcholine), (b) SM (surfactant mixture), and (c) EtoH (ethanol). Each Component was set at different ranges (low to high) by keeping the total composition at 100 %. PC, SM, and EtoH were coded as A, B and C, respectively, at the following ranges (A: 30–83 %), (B: 10–63 %), and (C: 7–10 %). Similarly, R_1, R_2, R_3, and R_4 were assigned for vesicle size, PDI, zeta potential, and %EE, respectively. The selected factor PC and SM served as the prime components of elastic liposomes. The level of each factor was decided as per the mixture design requirement (total composition 100 %) under the assumption that doubling each factor concentration while maintaining the same ratio (SM in 1:1) would not affect the responses (De Aguiar et al., 1995). At the beginning of trial running, several trail runs were suggested as shown in Table 2. Thus, the selected parameters (A, B, and C) were decided using information gained from the trial runs. The ratio (1:1) of span 80 and tween 80 (1:1) provided stable product than standalone (span 80 or tween 80). Ethanol was used for the membrane flexibility and it was required to optimize at optimal level. Formulation quality attributes were affected with the studied factors. Therefore, the optimized product was evaluated for size, morphology, and other characteristics. The generated polynomial equation was used explain the impact of each factor on responses and the program established cause-effect relationship within the experimental design space.

Desirability numerical parameters and other statistical analysis (analysis of variance, regression correlation, F, and p values) were determined using the program. Statistical parameters decided the best fit of the adopted model such as correlation coefficient (r^2), p and F values (Hussain et al., 2022; Gusai et al., 2020). The generated mathematical equations were interpreted based on the sign and coefficient value of each term. Graphical and numerical optimization process were assessed using individual (d_i) and overall desirability function (D_i). Therefore, any value near to one indicate the best fit of the model in the optimization process whereas the value near to zero represents a poor fit of the model. The predicted compositions of the optimized ketoconazole loaded cationic elastic liposome (OKEL1) were 80.78 %, 11.88 %, and 9.99 % for X_1, X_2, and X_3, respectively. The predicted Y_1, Y_2, and Y_3 values were 270 nm, 0.27, and 80.78 %, respectively, for the suggested compositions.

3.8. Formulations characterizations

3.8.1. Vesicles size, zeta potential, and PDI

Proposed formulations by the software were prepared and evaluated for vesicle size, PDI, and zeta-potential (ZP) as per the method described in earlier sections. ZP indicates the measure of charge density on the vesicle surface as required for the storage stability.

3.9. % Entrapment efficiency: %EE

For %EE, each formulation was separately studied. 10 mL of the test formulation was transferred into a centrifugation tube (plastic Falcon tube). The same tube was kept in the centrifugation slot along with blank tube (compensatory tube in the opposite side). The tube was ultra-centrifuged at 22000 rpm for 15 min to collect the settled vesicles pellet at the bottom. The supernatant was removed and saved for back calculation. The pellet was washed with distilled water and re-suspended in the water by mild probe sonication. The colloidal suspension of vesicles was passed through membrane filter (0.45 μm) to retained undissolved crystals of ketoconazole. The filtrate was collected and fractured using a mixture of organic solvents (chloroform and methanol) followed by stirring (magnetic stirring for 2 h). The mixture was again filtered and the filtrate was used to analyze the drug content entrapped in the vesicles. The supernatant was also used to estimate for the free drug content and back calculation using eq. (3).

$$\%EE = [(Q_t - Q_s)/Q_t)] \times 100 \quad (3)$$

where, Q_t and Q_s were total theoretical amount of the drug added and the amount of KETO found in the supernatant, respectively.

3.9.1. Desirability function: a numerical parameter

Desirability is a numerical function with an objective to reach the value of 1 or near to unity leading to the best fit under the set conditions of constraints and goals. The parameter can be used to identify interaction between factors if exists. Statistically, "D_i" is a geometrical mean function of all studied responses which depends upon the constraints and goals (maximum, minimum, in range and equal to, and target) set by the investigator for optimization (as shown in eq. 4):

$$D_i = (d_1.d_2.\ldots..d_n) = (\pi_{ii=1}\ d_i)^{1/n} \quad (4)$$

3.10. Evaluation of the optimized formulations

The optimized formulations were optimized and subjected for evaluations such as size, PDI, zeta potential, %EE, morphology using transmission electron microscopy (TEM), and % drug release profiles. Morphology of the optimized vesicles was assessed using a TEM technique. A sample was placed on the copper grid and allowed to be dried for overnight. Then, it was coated with gold followed by drying. The sample was visualized at varied resolution and power. The obtained

images were compared with the blank vesicles.

3.11. In vitro drug release profile

In vitro drug release study was conducted to investigate the behavior of the drug release in the PBS solution through a dialysis membrane of 12–14 K molecular weight cut-off (Sigma Aldrich, USA). A fixed dimension of the membrane was obtained and dipped into the PBS solution for 2 h. The activated dialysis membrane was used and one end was tightly closed using a thread. The other end was used to fill the sample (1 mL) and then it was tightly closed. The loaded dialysis membrane was dipped into the release medium (PBS of 250 mL) already set at fixed temperature (37 ± 1 °C) and stirring (100 rpm). Sampling was performed at varied time points (0, 0.5, 1, 2, 4, 8, and 12 h). The sample was analyzed using a UV vis spectrophotometer (Hussain et al., 2021). Various mathematical models were applied to investigate the release mechanism of the drug from the carrier.

3.12. Ex vivo permeation and drug deposition studies

To understand the extent of the drug permeation and deposition in the rat skin, it was required to perform ex vivo study for the formulations. Rats were issued from the institutional ethical committee (College of Pharmacy, King Saud University, Riyadh, approval no. KSU-SA-16-2020). Animals were randomly grouped for the control and the treated groups. These were housed in air conditioned room with the access of water and food. Then, they were quarantined for 12 h before experimental commencement. Abdominal skin was excised from rat after ethical sacrifice. The skin hairs were freed and the adhered fatty debris were removed using surgical stainless steel scalpel. Five groups were designated as A, B, C, D, and E for the control (untreated), DS, liposomes, OKEL1, and OKEL1-gel, respectively. The skin was mounted to Franz diffusion cell between the donor and the acceptor chambers. The acceptor chamber was filled with 22.5 mL of PBS and it contained a rice magnetic bead (Basu et al., 2018). The epidermis portion of the mounted skin touched the PBS solution. The epidermis section faced air to receive the test sample. The whole assembly was set at 37 ± 1 °C and 100 rpm. Sampling was carried out at different time points after 30 min of simulated temperature. Each sampling volume was replaced with fresh release medium. To maintain a sink condition, 5 % DMSO (dimethyl sulfoxide) was added in the PBS solution (pH 7.4). The permeated profiles (cumulative drug permeated, enhancement ratio, and targeted flux) and the deposited content were estimated using a validated method (Basu et al., 2018).

The drug deposition was conducted after completion of permeation study. At the end of 12 h, the mounted skin samples were removed and the exposed skin was excised. The adhered sample was gently removed using running water. The tissue was sliced into small pieces and the drug was extracted after stirring (12*h*) with methanol-chloroform mixture. The extracted drug was obtained after filtering the supernatant of centrifuged mixture through a membrane filter (0.45 μm). The total drug deposited was estimated and reported as percent.

3.13. Statistical analysis

Experiments were repeated to express the result as mean with standard deviation ($n = 3$). Statistical analysis was carried out in the experimental design to select the right model and success of the optimization process. A significance difference in data was considered at p value below 5 % as compared to the control. Few statistical model such as "Kruskal-Wallis analysis" and Denn's test" were used wherever required. Regression coefficient analysis was studied using Microsoft excel for linear graph construction. However, regular, predicted and adjusted r^2 were obtained using Design Expert software.

4. Results and discussion

4.1. HSPiP based predicted theoretical solubility in the excipients

HSPiP provided various HSP values for the drug and excipients required to formulate cationic elastic liposomes for topical delivery of ketoconazole as shown in Table 1 and Fig. 1A. The drug is highly lipophilic as evidence with the high values of δ_d (21.6 $MPa^{1/2}$), δ_p (11.9 $MPa^{1/2}$), and logP (4.3). These values can be correlated to the chemical structure of ketoconazole (five rings with least number of polar functional groups) and the lack of hydrogen bonding donor counts (Fig. 1B). The literature based values of δ_d, δ_p, and δ_H are 16.1 $MPa^{1/2}$, 6.4 $MPa^{1/2}$, and 9.1 $MPa^{1/2}$, respectively. Considering the δ_d values of the drug and PC, the lipophilic lipid bilayer is expected as the prime of the drug lodging (lipid-lipid amalgamation via dispersion energy). The drug was expected to be highly soluble in chloroform as compared to methanol. This can be rationalized based on the HSP difference between the solute and the explored solvent (Yoshihara, et al., 1986; Hansen, 2007). These differences are quite small such as $\Delta\delta_d$ (4.0 $MPa^{1/2}$), and $\Delta\delta_H$ (0.1 $MPa^{1/2}$). Thus, hydrogen bonding interaction may predominantly work to solubilize the drug in chloroform over polarity and dispersion (hydrocarbon moiety) energies. However, this was further simulated by performing experimental study in the same solvent. In case of surfactant, lipophilic span 80 was predicted to be better than hydrophilic tween 80 which may be due to hydrophobic nature of the drug and the closeness of HSP values between ketoconazole and span 80 (HLB = 3.4). Thus, theoretical predicted qualitative solubility of the drug based on HSP values of the drug, ethanol, PC, and span 80, a suitable formulation may be fabricated using these excipients. Lipophilic SA was least in quality and therefore, it was expected to have insignificant impact on the drug solubility in the lipid bilayer. It was used as cationic charge inducer (Vassoudevane et al., 2023). Chemically, the drug is an azole antifungal compound bearing zero H-bonding donor counts, six H-bonding acceptor (HBA) counts. The π-π interaction (London dispersion force) can be possible reason for improved solubility in the excipient (Yoshihara and Nakae, 1986; Abbott, 2010).

4.2. Differential scanning calorimeter (DSC)

The result of thermal behavior of the drug and excipients are presented in Fig. 2A-D. The technique determined the fusion temperature (a sharped endothermic peak) of PC as 70.8 °C which is in good agreement with the reported finding (66.56 °C) with slight variation as shown in Fig. 2A (Nakamura et al., 2017). SA exhibited characteristic endothermic peak at 56.6 °C suggesting crystalline nature of the solid state and saturated long hydrocarbon chain stacked together to render highly compact packing of the molecules in lattice crystals (Fig. 2B) (Semalty and Tanwar, 2013). Moreover, the physical mixture (PM) revealed a sharp endothermic peak at 74.66 °C followed by the absence of the drug characteristic peak (generally observed at 146–150 °C) as shown in Fig. 2C. A remarkable intense endothermic peak of the drug at 146.9 °C suggested the purity of the compound without thermal degradation studied at the explored temperature range (30–357 °C). The absence of the drug peak from PM may be attributed to the amalgamation of the drug in the PC after fusion (Fig. 2C and Fig. 2D).

4.3. Experimental solubility of KETO in the predicted solvents

Experimental solubility (mole fraction solubility) of the drug was investigated in PC, chloroform, span 80, tween 80, distilled water and ethanol. The drug is categorized under the BCS II (biopharmaceutics classification system) due to limited aqueous solubility (17 μg/mL) at room temperature (Kumar et al., 2018). This finding was in good agreement with our result (23.4 ± 0.4 μg/mL) in the distilled water. The experimental solubility values of the drug in the explored excipients were found to be as 4.7 ± 1.6 mg/mL, 7.9 ± 0.08 mg/mL, 19.9 ± 1.94

Table 1
HSPiP software based predicted excipients based on HSP values for KETO.

Name		HSP values estimated					
Excipients	Ra estimated	δ_d ($MPa^{1/2}$)	δ_p ($MPa^{1/2}$)	δ_H ($MPa^{1/2}$)	δ_t ($MPa^{1/2}$)	M. vol	RED
KETO	Predicted solubility (%*w*/w) @45 °C	21.6	11.9	6.2	25.4	390.0	–
Methanol	8.23	16.4	12.3	21.7	29.9	41.1	2.0
Sodium cholate	–	17.6	5.9	9.8	21.0	389.3	1.0
Water	0.0034	15.6	16.0	42.0	47.6	18.0	3.95
Chloroform	2.34	17.6	5.8	6.3	19.5	75.5	1.08
Stearylamine	–	16.0	1.8	3.4	16.5	329.5	1.64
PC*	–	16.1	6.4	9.1	25.01	–	1.35
Span 80	0.61	16.6	5.6	7.5	19.1	429.2	1.27
Tween 80**	0.33	19.0	5.3	5.6	20.5	20.0	0.91
Ethanol	5.86	15.6	9.3	17.2	25.0	58.2	1.77
OKEL1	20.0	–	–	–	–	–	–
Ro – Ra is needed for the fit function							
	SMILE						
KETO	CC(=O)N1CCN(CC1)c2ccc(cc2)OC[C@H]3CO[C@](O3)(Cn4ccnc4)c5ccc(cc5Cl)Cl						
Methanol	"CO"						
Sodium cholate	C[C@H](CCC(=O)[O-])[C@H]1CC[C@@H]2[C@@]1([C@H](C[C@H]3[C@H]2[C@@H](C[C@H]4[C@@]3(CC[C@H](C4)O)C)O)O)C						
Water	"OH"						
Chloroform	C(Cl)(Cl)Cl						
Stearylamine	CCCCCCCCCCCCCCCCCCN						
PC	C[N+](C)(C)CCOP(=O)(O)OCC(COC=O)OC=O						
Span 80	CCCCCCCCC=CCCCCCCCC(=O)OCC(C1C(C(CO1)O)O)O						
Tween 80	CCCCCCCCC=CCCCCCCCC(=O)OCCOCC(C1C(C(CO1)OCCO)OCCO)OCCO						
Ethanol	CCO						

* (Prasanthi and Lakshmi, 2012).

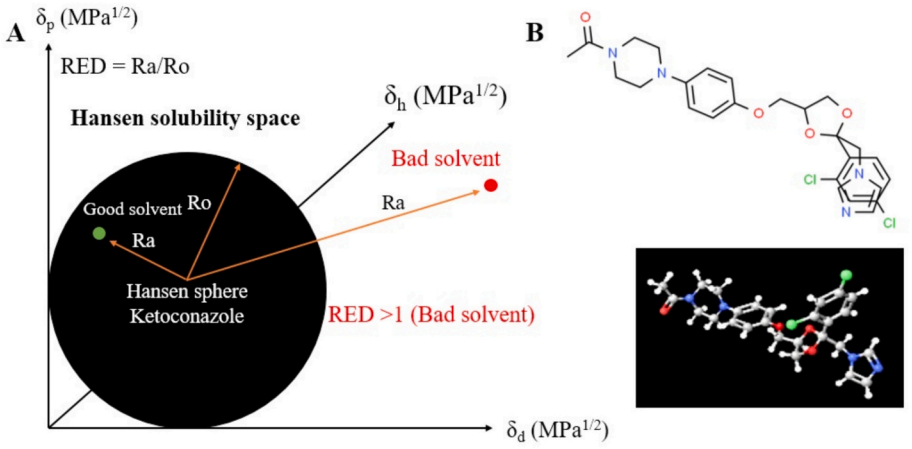

Fig. 1. (A) Hansen solubility sphere with three different solubility parameters in Hansen space and (B) Ketoconazole structure possessing various Hydrogen bond donor and acceptor counts.

mg/mL, 11.3 ± 0.6 mg/mL, and 18.7 ± 0.13 mg/mL in ethanol, methanol, chloroform, span 80, and tween 80, respectively at the studied temperature (Sodeifian et al., 2021). The established correlation between the predicted and actual solubility of the drug in water, chloroform, S80, and tween 80 was 0.65. Positive correlation suggested good correlation and positive slope of correlation curve. In the similar way, the established correlation was 0.94 for water, chloroform, and span 80. In contrast, a poor correlation was obtained between the actual and predicted solubility values obtained methanol and ethanol which resulted in negative correlation (− 0.21) among explored size solvents. This can be due to the predicted value at high temperature (45 °C) for the highly volatile solvents such as methanol and ethanol.

The obtained results showed that water executed the least solubility due to lipophilic nature of ketoconazole (high δ_d value) and maximum in tween 80. The highest mole fraction solubility of the drug may be attributed to high dispersion energy (δ_d = 19.0 $mMPa^{1/2}$) and maximized polarity interaction (δ_d = 5.6 $mMPa^{1/2}$) (Table 1). These interactions are in close to the HSP values of the drug resulting in low value of their respectively differences. The low the difference of the respective HSP value, the more is expected to be soluble (Yoshihara et al., 1986).

4.4. Preparation of various trial formulations and characterized parameters

Several products were formulated by varied content of span 80, tween 80, and PC. However, the content of ethanol and SA were kept constant. Formulations containing tween 80 found to be unstable on standing for benchtop stability overnight at room temperature. Therefore, span 80 based formulations (2 %*w*/w) were formulated to load the required dose (20 mg) of the drug. Table 2 summarized the composition of span 80 based trial formulations. ST served as positive charge inducer to get cationic elastic liposomes whereas ethanol was used to render ultra-deformability, flexibility, and elasticity in the lipid bilayer of vesicles.

Formulations (S1– S9) were characterized for vesicle size, PDI, zeta potential, and % EE values. Result is present in Table 2. The vesicle size, PDI, zeta potential, and %EE values were found in the range of 247–775

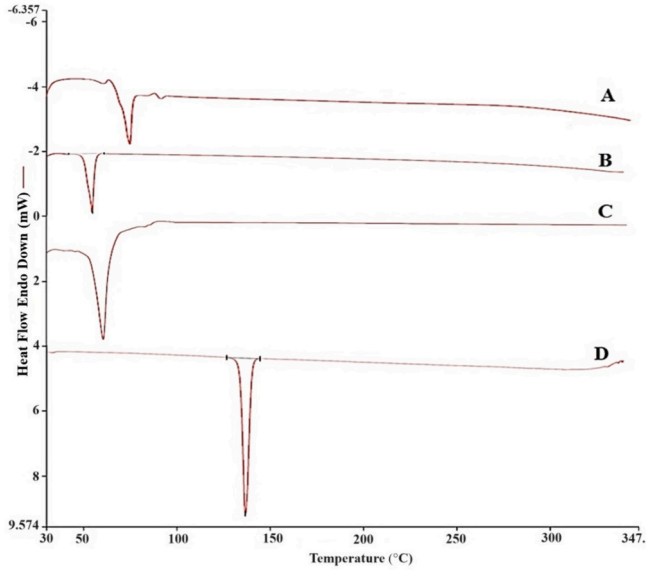

Fig. 2. Thermal behavior of the drug and excipients determined using DSC (differential scanning calorimeter): (A) PC (70.8 °C), (B) stearylamine (56.06 °C), (C) physical mixture (the drug and excipients) (74.66 °C), and (D) Ketoconazole (146.9 °C).

Table 2
Each mL of the formulation contains the following composition.

Formulation	PC (mg)	S80 (mg)	SA (mg)	PBS (mL)	Ethanol (mg)	Stability (24 h)
S1	50	50	5	1	70	stable
S2	60	40	5	1	70	stable
S3	70	30	5	1	70	stable
S4	85	15	5	1	70	stable
S5	90	10	5	1	70	stable
S6	40	60	5	1	70	stable
S7	30	70	5	1	70	stable
S8	75	25	5	1	70	stable
S9	80	20	5	1	70	stable

	Characterized parameters				
Formulation	Size (nm)	PDI	Zeta potential (mV)	% EE	Shape
S1	329	0.35	+ 23.6	36.8	Spherical
S2	266	0.54	+ 26.1	54.9	Spherical
S3	337	0.48	+ 25.2	67.9	Spherical
S4	271	0.36	+ 27.7	84.2	Spherical
S5	775	0.43	+ 25.5	32.6	Spherical
S6	375	0.48	+ 29.3	58.1	Spherical
S7	249	0.37	+ 22.1	29.7	Spherical
S8	312	0.45	+ 30.4	72.9	Spherical
S9	247	0.53	+ 27.3	40.2	Spherical

Note: SA = stearylamine, S80 = span 80, PC = phosphatidylcholine, PBS = phosphate buffer solution, PDI = Polydispersity index, %EE = Percent entrapment efficiency.

nm, 0.35–0.54 nm, 22.1–30.4 mV, and 29.7–84.2 %, respectively as shown in Table 2. Formulation S4 was associated with the optimal values of vesicle size (271 nm), PDI (0.36), high zeta potential (~ 28 mV), and the highest values of %EE (84 %). This may be attributed to optimal ratio of PC to span 80. The maximum vesicle size of S5 can be justified based on the highest content of PC (90) with respect to span 80 (low content leading to insufficient emulsification and vesicle generation during hydration stage) (Hussain et al., 2021). The drug is lipophilic and the lipid bilayer of vesicle is the lodging place as result of lipid-lipid interaction (amalgamation). Therefore, from S1 to S4, there were progressive increase in %EE with increase in PC content in the formulation (Table 2). Beyond S4, there was sudden reduction in %EE due to high content of PC with respect to span 80. The optimized formulation S4 was scanned under TEM to confirm morphology. Fig. 3A-B exhibited spherical behavior of S4 under TEM. In Fig. 3A, the vesicles were found to be well dispersed without any aggregation whereas S5 revealed significant aggregation and irregular shape resulting in significantly high vesicle size (775 nm) (Fig. 3B). This difference may be due to the large content of PC in S5 as compared to S4 as consequence of insufficient emulsification. The estimated fold error for the estimated size of both formulations were found to be below 2 suggesting acceptable instrumental error in size analysis using TEM and DLS techniques (Hussain et al., 2021).

4.5. Optimization using design expert

DoE established a relationship between factors and studied responses followed by finding the impact of each factor on response. Moreover, each factor was separately processed for statistical best fit of the model. D-optimal design is a model dependent, straight forward, limited runs required, the constrained design space, minimize the overall variances, and effects estimates are correlated (Patel et al., 2010; De Aguir, et al., 1995). Here, three components (A, B, and C) were studied within specific ranges where their combined total equals to 100 %. The factors and their levels were decided based on the estimated size, PDI, ZP, and %EE values obtained from trial batches. PC, SA, and EtoH (ethanol) were designated as A, B and C, respectively, at the following ranges (A:30–83 %), (B:10–63 %), and (C:7–10 %) in the selected mixture mode. Thus, PC (A), SM (B), and ethanol (C) were three prime factors against four responses namely, vesicle size (R_1), PDI (R_2), ZP (R_3), and %EE (R_4) (see Table 2). Formulations (1−12) were proposed by the software and the FDS (fraction design space) value (mainly size and %EE) > 80 % allowed the design to have enough power to utilize the data for the most optimized formulation (Zen et al., 2015). Total of 12 products were evaluated for size, PDI, ZP, and % EE values. Results are presented in Table 3. The vesicle size, PDI, zeta potential, and %EE values were found in the range of 164–950 nm, 0.27–0.85, 21.0–33.8 mV, and 49.9–83.9 %,

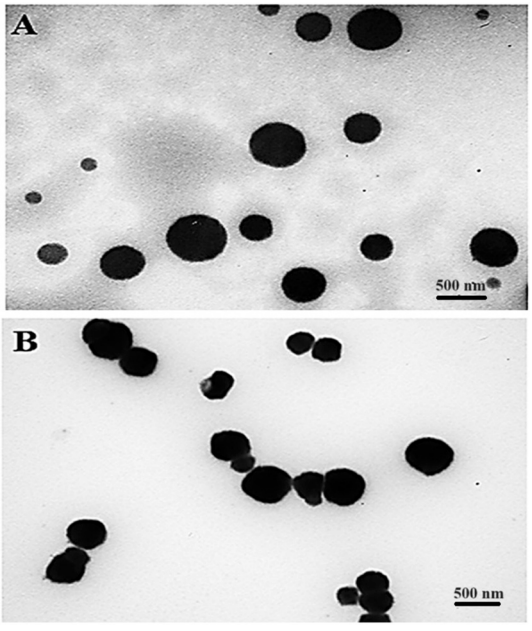

Fig. 3. Representative microphotographs of S4 and S5. (A) Apparently dispersed and spherical morphology (shape) of S4 suggesting stable and low PDI and (B) vesicles of S5 with slight deviation from spherical shape (aggregation observed). Magnification at 50000 X.

Table 3
Experimental design (optimal custom design) using Design Expert (mixture mode), and summary of optimization input parameters.

	Levels			Responses			
	-1		+1	Y_1	Y_2	Y_3	Y_4
A: PC (mg)	30		83	Size (nm)	PDI	zeta potential (mV)	% EE
B: SM* (mg)	10		63				
C: Ethanol (%)	7		10				
Constraints				minimum	minimum	maximum	maximum
Importance				+++	++	+++	+++
Run	A	B	C	Y_1	Y_2	Y_3	Y_4
1	51	42	7	875	0.851	23.5	42.9
2	31	61	8	243	0.348	26.7	63.2
3	45	45	10	164	0.269	33.8	65.8
4	43	50	7	283	0.471	21.0	70.4
5	82	10	8	553	0.543	27.3	77.5
6	58	33	9	918	0.306	31.6	52.8
7	70	23	7	418	0.559	22.5	83.9
8	31	61	8	281	0.405	26.9	61.4
9	79	11	10	256	0.406	25.7	73.7
10	58	33	9	929	0.371	28.4	59.2
11	58	33	9	950	0.351	27.1	53.0
12	38	52	10	212	0.457	30.4	59.7
Liposomes	Lipid	SM	Cholesterol	Y_1	Y_2	Y_3	Y_4
	75	20	05	178.4	0.374	- 22.9	59.5

* SM: surfactant mixture (1:1).

respectively as shown in Table 3. Formulation S4 was associated with the optimal values of vesicle size (271 nm), PDI (0.36), zeta potential (~ 27.7 mV), and the highest values of %EE (~ 84.2 %). This may be attributed to optimal ratio of PC to SM. S5 was associated with the largest particle size (775 nm) which can be due to particle aggregation as evidenced with the TEM report (Fig. 3B). Thus, particle aggregation resulted in low drug entrapment and instability on benchtop storage stability.

4.6. Evaluated parameters

4.6.1. Vesicle size (nm): R_1

The size of an elastic liposomal formulation is a critical parameter when developing formulations for topical or transdermal applications. However, cationic elastic liposomes exhibit unique characteristics compared to conventional liposomes. These vesicles are capable to be deformed under stress, adaptable, to be squeezed into deeper skin layer, and water gradient based permeation across stratum corneum (Ba-Abbad et al., 2013). The generated mathematical model for R_1 presented in Tables 3 and 4. Vesicle size ranged as 164–950 nm and quadratic equation was R_1:119.75 A – 64.33B-490300C + 2486.47AB + 521,500 AC + 515,200 BCE. Fig. 4A elicited 3D response surface for three factors against R_1 with maximum optimal at top. The best fit model was quadratic considering ANOVA (analysis of variance) data (p as 0.015, F as 7.4, and r^2 as 0.86) (Table 4). The components (A, B and C) showed substantial impact on the size ($p < 0.05$) wherein the mid-range of component C was preferred.

Table 4
Summary of statistical models and parameters.

Response	Model	p	F	R^2	Adjusted R^2	PRESS
R_1	Quadratic	0.015	7.44	0.86	0.75	1,655,000
R_2	Special quadratic	0.011	25.53	0.98	0.95	0.417
R_3	Linear	0.0085	8.49	0.65	0.58	111.4
R_4	Special quadratic	0.016	20.29	0.98	0.93	1989.39
	Generated polynomial equations					
R_1	119.75A – 64.33B – 490300C + 2486.47AB + 521,500 AC + 515,200BC					
R_2	– 0.6094A– 0.7822B – 983.57C + 6.54AB + 1064.11 AC + 1060.30BC– 433.60A^2BC – 185.75AB^2C + 2211.55ABC^2					
R_3	22.09A + 24.24B + 158.29C					
R_4	198.16A + 171.66B + 98,673.81C– 582.13AB – 106,900 AC-106000BC + 34,688.45A^2BC + 18,760.40AB^2C – 234100ABC^2					

4.6.2. PDI: R_2

Polydispersity index is an indication of the broadness of the size-distribution within a specific formulation. Lower values indicate a monodispersed sample while the value >0.7 indicates heterogeneous nature of dispersed vesicles. At all mixture component ratios of (12 runs) formulations showed values in the range of 0.27–0.85. Special quadratic model for R_2 was obtained as $R_2 = -0.6094$ A – 0.7822B – 983.57C + 6.54AB + 1064.11 AC + 1060.30 BC – 433.60A^2BC – 185.75 AB^2C + 2211.55ABC.^{2} Fig. 4B showed the response surface plot of R_2. Special quartic equation was the best fit model based on ANOVA report and showed p (0.011), F value of (25.5), and r^2 value of 0.98 (Table 4).

4.6.3. Zeta Potential: R_3

Zeta potential is an electric difference between vesicle and media. Positive or negative values indicate stability of the product (21–33.8 mV). Linear model was generated as $R_3 = -22.09$A + 24.24B + 158.29C. Fig. 4C showed the response surface plot of R_3. Linear equation was the best fit model based on ANOVA report and showed p of 0.009, F value of 8.5 and r^2 value of 0.65 (Table 4). The generated equation of R_3 on mixture components (A, B and C) elicited that ZP significantly ($p < 0.05$) rises with decrease in C and any A or B ratios. The values of the ZP are expected to be positive due to the use of SM. Thus, the more positive value the better is stability.

4.6.4. % Entrapment efficiency: R_4

Hydrophobic KETO (log P of 3.5) was considered to be preferentially lodged into the lipophilic lipid bilayer. Therefore, %EE were varied from 49.9 % to 83.9 % as shown Table 3. Here, the %EE varies with different ratios of the selected components. Software generated mathematical special quadratic equation of $R_4 = 198.16$ A + 171.66B + 98,673.81C – 582.13AB – 106,900 AC – 106,000BC + 34,688.45A^2BC + 18,760.40AB^2C – 234100ABC^2 (Table 4) is the best fit model as evidence with p (0.016) and F (20.29) values. Fig. 4D depicted the 3-D surface plot of R_4 against A, B and C. ANOVA analysis report found a good agreement between the adjusted r^2 (0.98) and predicted r^2 (0.93) indicating a good fit of the quadratic model.

Correlation curves for R_1, R_2, R_3, and R_4 between the predicted and the actual values are illustrated in Fig. 5A-D. There was a good correlation as evidence with the high linear regression coefficient ($r^2 > 0.98$).

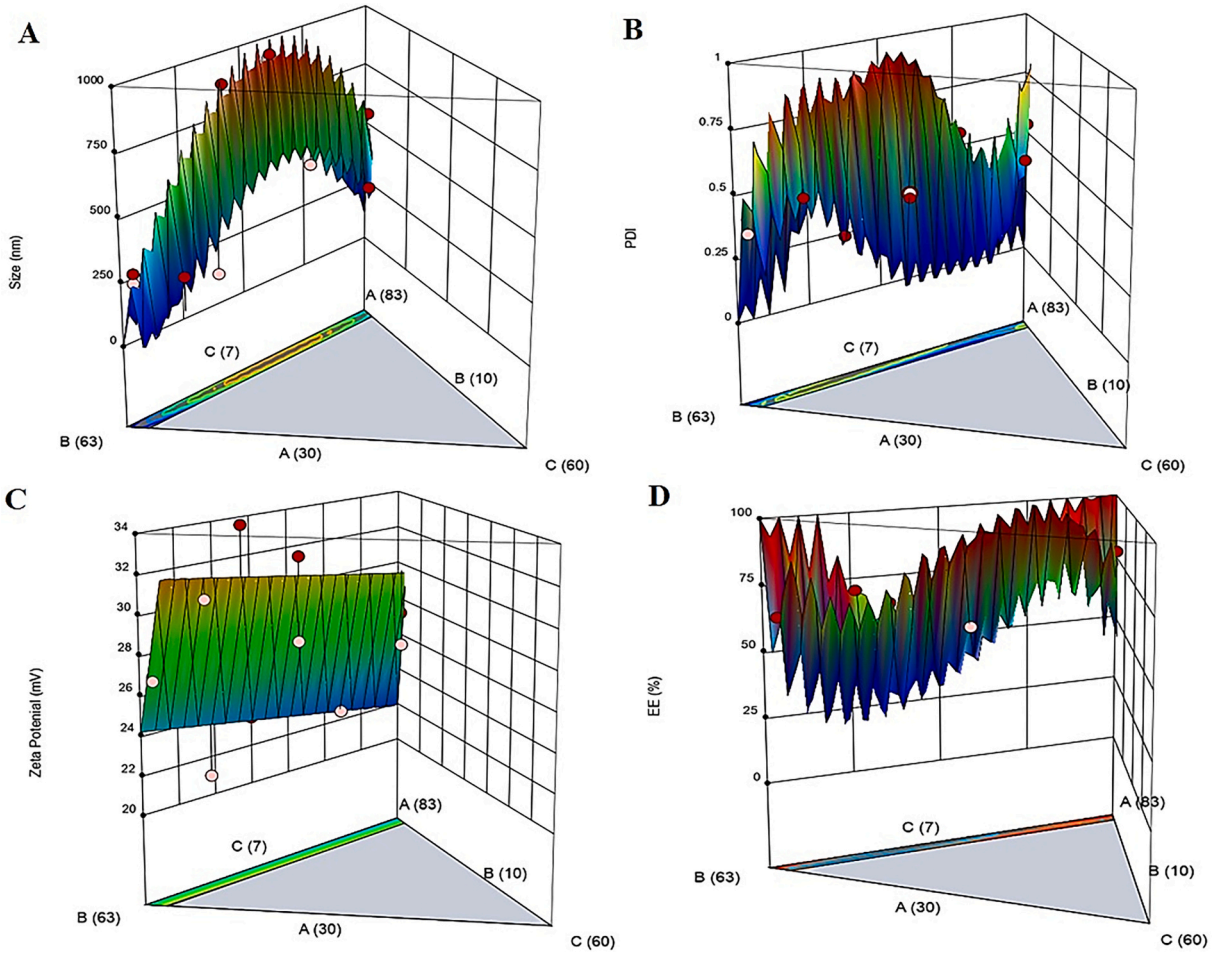

Fig. 4. 3-dimensional response plots obtained from optimization: (A) Size as R_1, (B) PDI as R_2, (C) Zeta potential as R_3, and (D) %EE (R_4).

4.6.5. Desirability

This numerical objective function is applied for validation of the optimization process. Here, the optimized formulations are identified under specific set of constraints and importance given to the independent and dependent variables. This function suggested 8 formulations with specific ratios of A, B and C. Experimental values of vesicle size, PDI, and %EE for optimized formulation with desirability function values of 0.91 is observed as shown in Fig. 6A. The observed values were found to be in agreement with predicted values suggesting the best fit of the model. This desirability indicated the suitability of the model for optimization process. Fig. 6B revealed the optimized composition of OKEL1 and predicted size (270 nm), PDI (0.27), and %EE (80.78 %).

4.7. Summary of statistical analysis

Table 4 summarized the statistical report of optimization. R_1, R_2, R_3, and R_4 followed quadratic, special quadratic, linear, and special quadratic, respectively. It is clear that R_3 exhibited the least value of regression coefficient (r^2) as compared to others. This may be attributed to constant amount of SA in the formulation. The impact of SA on zeta potential was found to be weakly related due to constant content. However, overall impact of observed to be linear. Higher the SA content, higher the ZP (positive) would be achieved.

4.8. Evaluation of the optimized formulation (OKEL1) and OKEL1-Gel

Post-optimized formulation OKEL1 was characterized for vesicle size, zeta potential, and PDI. The experimental actual values of size, ZP, and PDI were found to be as 259 nm, +2.4 mV, and 0.24, respectively. These values were closely related to the predicted values of vesicular size (270 nm) and PDI (0.27). The experimental value of %EE was estimated as 83.1 %. For gel formulation, the sample was diluted with distilled water before size analysis. The vesicle size and size distribution change values (252.9 nm and 0.21 mV) were found to be insignificant after incorporating into the gel matrix. Cationic liposomes The slight decline in zeta potential value (0.21 mV) may be attributed negatively charged carboxylic nature of monomer matrix responsible to interact with cationic liposomes surface (adsorption phenomenon) (Franzé et al., 2017).

4.9. FTIR study: Compatibility study

It is required to assess compatibility of the drug with excipients. Therefore, FTIR technique was employed to observe possible functional group bond vibration and bond stretching among them. Fig. 7A portrays pure compound FTIR with characteristic peaks as the fingerprint of ketoconazole. The drug exhibited remarkable peaks at 3098.82 cm^{-1}, 2936.14 and 2732.09 cm^{-1} due to N—H and aliphatic C—H stretching, respectively. Moreover, intense absorption peaks detected at 1743.53 and 1689.53 cm^{-1} were related to carbonyl group (C=O) for stretching vibration. Two characteristic peaks at 1631.06 cm^{-1} and 1245.5 cm^{-1}, are revealed due to aromatic ring of the drug and C—O bond vibration, respectively. These peaks confirmed the purity of the compound and free from any contamination. Fig. 7B executed two prominent absorption peaks at 3397.7 and 1617.4 cm^{-1} due to N—H stretching and bending modes, respectively, present in SA. Two intense and sharp absorption

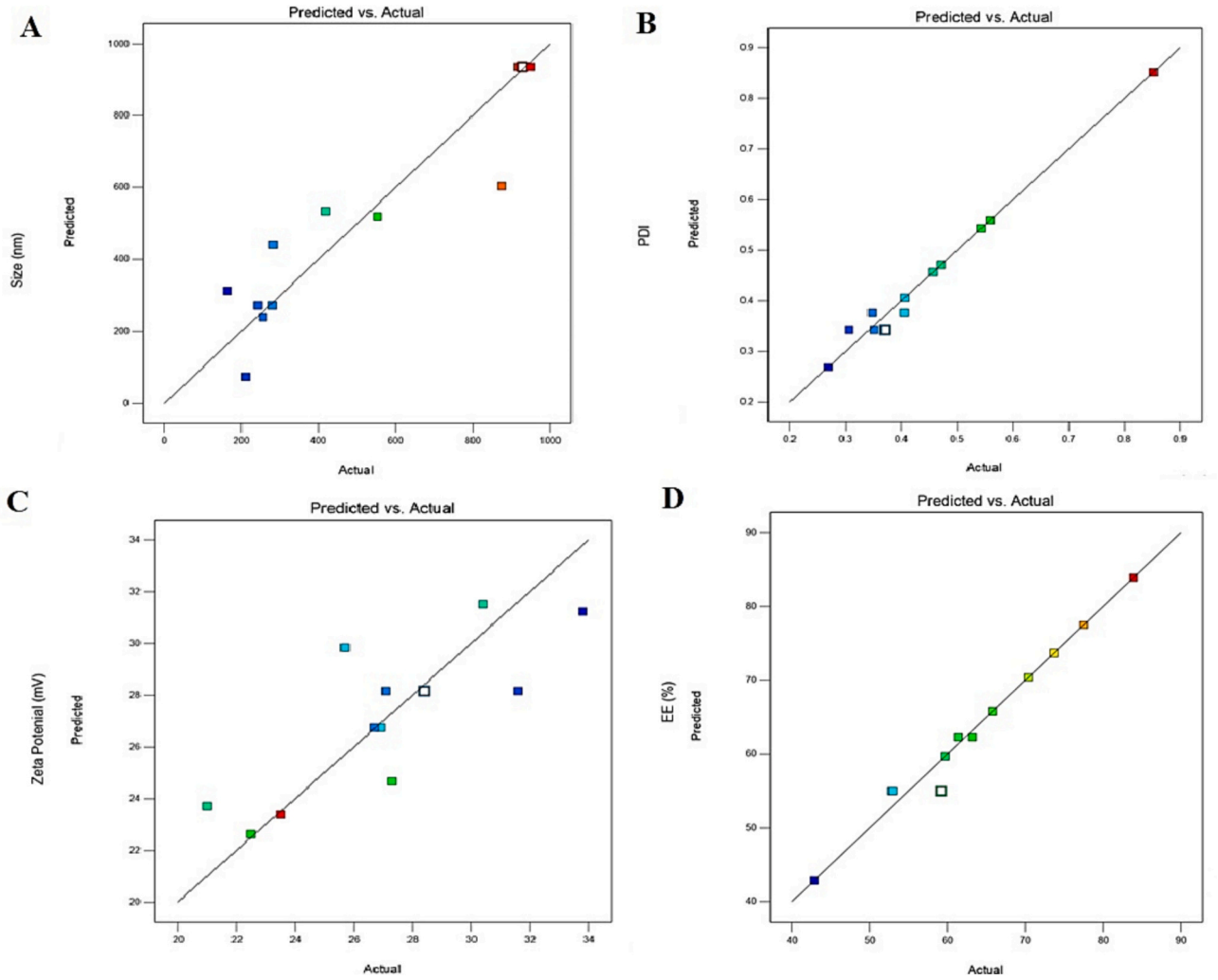

Fig. 5. Predicted versus actual correlation graph obtained from optimization: (A) Size as R_1, (B) PDI as R_2, (C) Zeta potential as R_3, and (D) %EE (R_4).

peaks were obtained at 2718–2882.7 cm^{-1} due to the C—H and = C–H stretching vibrations, respectively. It is noteworthy that mild characteristic peaks of ketoconazole obtained at 3098.82 cm^{-1}, 2936.14 and 2732.09 cm^{-1}, are merged with intense peak of SA scanned at 2718–2882.7 cm^{-1} as shown in physical mixture (Fig. 7C). Moreover, C—N and C—H bending vibrations were exhibited at 1467 and 1073 cm^{-1}, respectively, in SA. These finding were in good agreement with the published report with similar pattern and magnitude (Faria et al., 2019). The physical mixture (PM) of the drug and SA showed retained characteristic absorption peaks of the drug and excipients suggesting chemical compatibility among them (Fig. 7C). However, these characteristic peaks of the drug were completely absent in OKEL1 formulation due to the drug entrapment and insufficient amount of the drug unentrapped or adsorbed (Fig. 7D). A prominent absorption peak at 1617.4 cm^{-1} is related with N—H bending vibration in SA which persisted in OKEL1 due to successful lodging of SA in lipid bilayer. In OKEL1, it was slightly shifted to 1658.3 cm^{-1} which may be due to change in vibration within lipid bilayer integrity. Interestingly, the peak intensity was approximately unchanged due to constant concentration.

4.10. *In vitro drug release profile*

Result is revealed in Fig. 8. The drug suspension exhibited limited solubility (< 21 % at 12 h) and dissolution in the release medium due to high lipophilic nature (log $P = 4.3$) (Hussain et al., 2021). The in vitro drug release profile of DS showed approximately 20.7 ± 1.16 % drug release at the end of 12 h under the provided experimental conditions. This can be correlated to poor aqueous solubility, weak hydrogen bonding with water, and the drug precipitation at the explored temperature. Thus, limited ketoconazole from aqueous conventional cream is available as soluble form for permeation across the upper skin layer. The optimized formulation OKEL1, liposomes, and OKEL1-G were expected to elicit slow and sustained drug release behavior due to the lipid bilayer of the vesicles (liposomes and elastic liposomes) and viscous gel matrix (Lin et al., 2019). The lipophilic ketoconazole release from OKEL1 was greater than 83.3 ± 4.2 % at 12 h whereas OKEL1-G was found to execute extended drug release (63.7 ± 4.0 % over period of 12 h). This can be attributed to the difference between lipid bilayer compositions, and the effective diffusion double barriers (both gel and vesicular lamellae of OKEL1) (Blume and Cevc, 1990). Notably, OKEL1 exhibited the highest ketoconazole release from the trapping lipid bilayer of vesicles which may be related to its solubilized form available in the lipid bilayer and the surfactants mediated stable solubility maintained in the medium. This property may be helpful for the permeation across skin for slow and sustained drug delivery. The gel carrier of OKEL1 further slowed down its release due to viscosity mediated mitigated diffusion of vesicles in the matrix towards the membrane. However, the gel matrix may improve ex vivo permeation at the skin surface due to hydration. Thus, slow release of the drug from the gel matrix is due to viscosity. Moreover, the release mechanistic insight was investigated by applying Higuchi and Korsmeyer-Peppas model. Vesicular systems exhibited non-Fickian diffusion as evidence with $n \geq$

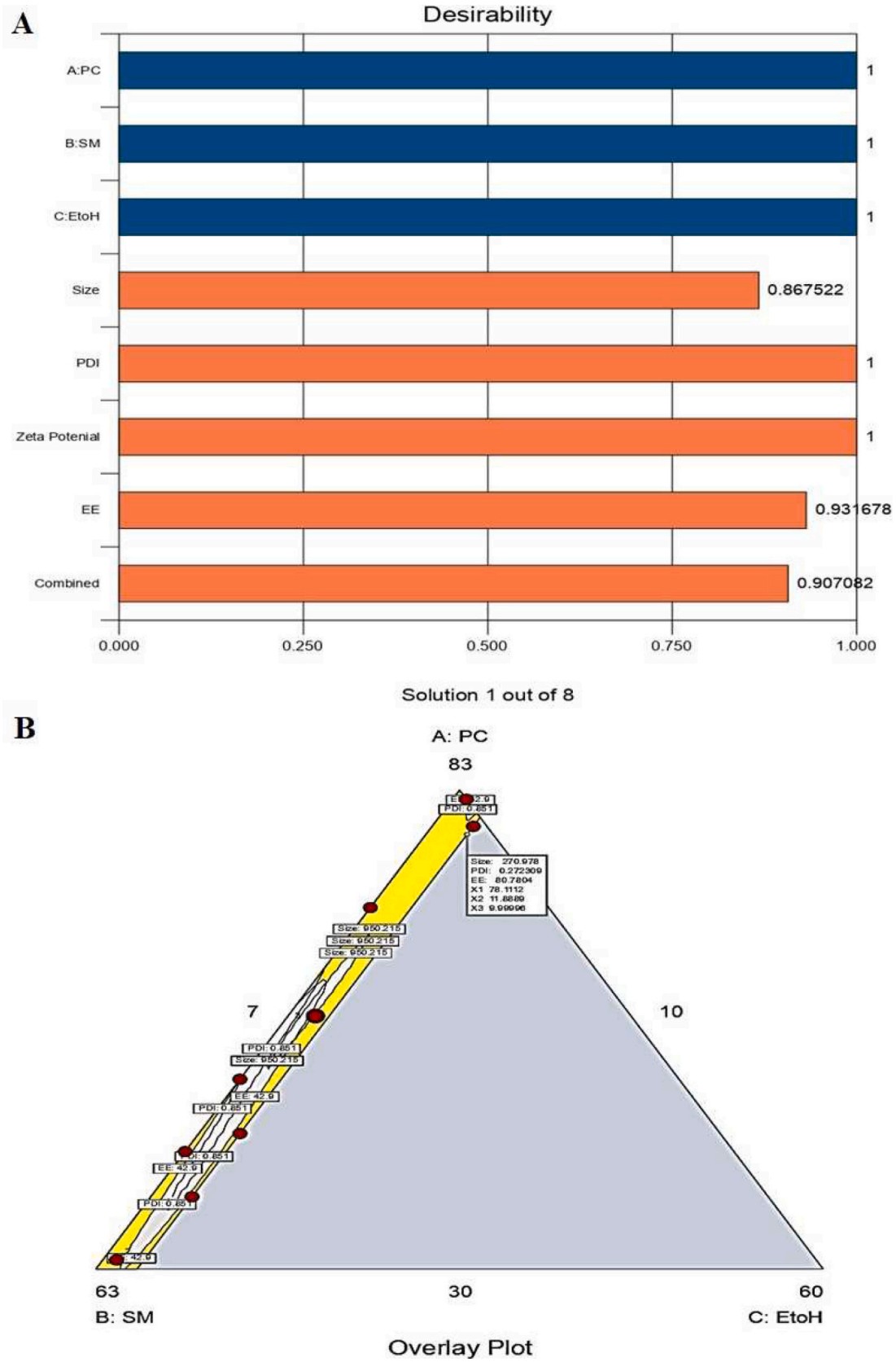

Fig. 6. Desirability and overlay plot: (A) Overall desirability as bar plot and (B) ternary diagram of overlay plot.

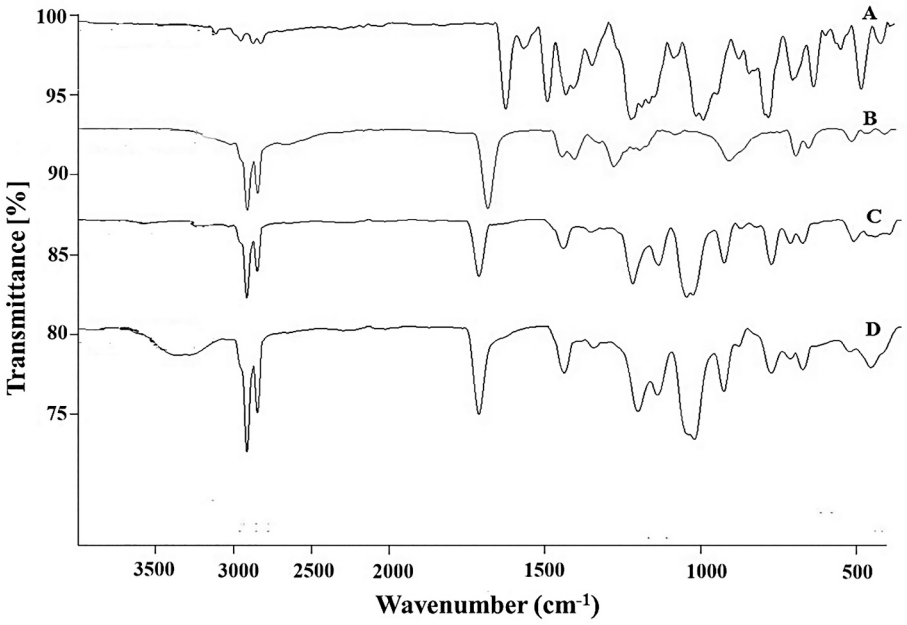

Fig. 7. FTIR study: (A) KETO, (B) SA, (C) PM, and (D) OKEL1.

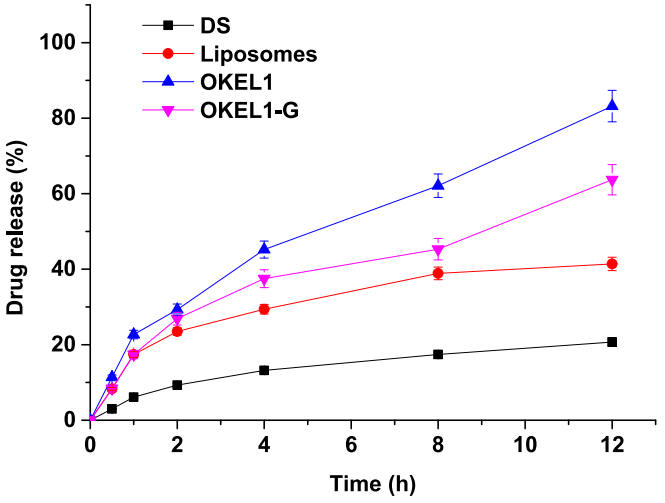

Fig. 8. In vitro drug release of ketoconazole from various formulations in phosphate buffer solution at 37 °C (mean ± standard deviation).

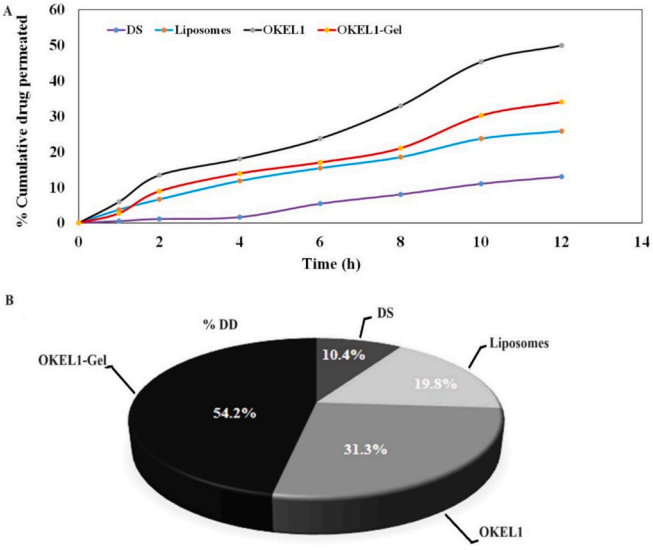

Fig. 9. (A) % cumulative drug permeated (per cm^2) and (b) % drug deposited (%DD).

0.5 (calculated for OKEL1, liposomes, and OKEL1-G). The obtained slow and non-Fickian diffusion can be explained based on the lipid bilayer of vesicle loaded with lipophilic ketoconazole.

4.11. Ex vivo permeation and the drug deposition studies

A comparative permeation behavior of DS, liposomes, OKEL1, and OKEL1-Gel was investigated across rat skin as shown in Fig. 9A. Percent cumulative drug permeated values were found to be 13.0 %, 25.8 %, 49.9 %, and 34.1 % from DS, liposomes, OKEL1, and OKEL1-gel at the end of 12 h, respectively. As expected, limited in vitro drug release profile (20.7 %) of DS suggested that it may execute poor permeation across skin surface due to limited aqueous solubility of the drug. OKEL1 and DS exhibited the highest (4.2 μg/cm^2.h) and the lowest values of permeation flux (4.15 μg/cm^2.h versus 1.08 μg/cm^2.h). The enhancement ratio for OKEL1 and OKEL1-Gel were obtained as 3.8 and 2.5 which may be attributed to vesicular mediated improved permeation and gel based compensated trans epidermal water loss in the skin resulting swelling and reversible perturbation in surface structure (Schlich et al., 2022). Liposomes exhibited limited enhancement ratio, permeation flux, and permeation coefficient as compared to its counter parts (OKEL1 and OKEL1-Gel) which may be due to cholesterol based rigid nature of liposomal vesicles and the lack of SA mediated cationic charge responsible for electrostatic interaction with cellular surface as observed in OKEL1 and its gel. SA played dual functionalities such as vesicle stability (pKa < pH for preferred ionizable cationic lipid less than physiological pH) at pH 7.4 and improved electrostatic interaction with negatively charged corneocytes of skin for improved permeation of ketoconazole (Kircik, 2012). Permeation coefficients values estimated were found as 0.00054, 0.001, 0.0021, and 90.0014 cm^2/h for DS, liposomes, OKEL1, and OKEL1-Gel, respectively. It is apparent that permeation coefficient of OKEL1 was 2.1 folds higher than the liposomes and 3.9 folds higher than DS.

The values of % DD have been illustrated in Fig. 9B. OKEL1 was

capable to enhance the drug deposition as compared to DS and the liposomes. However, gel results in further improved drug deposition which may be attributed to hydration mediated swelling (high drug diffusion through hydrated skin) and the compensated trans epidermal water loss (Ha et al., 2023; Cheng et al., 2023). Moreover, vesicular deformability, vesicle-skin interaction, vesicle squeezing ability through minute physiological pores of the skin, and developed concentration gradient worked in tandem for enhanced drug permeation and subsequently deposition (Slavkova et al., 2023). In general, greater the deposition, the greater would be expected to serve as deport within subcutaneous area for slow and sustained delivery of ketoconazole for effective and efficient therapeutic benefits (Hussain et al., 2017). Superficial fungal infections are easily treated using conventional liposomes and cream. However, it is challenging to treat deeply seated invasive dermal strains of *Aspergillosis* and *Candida* (resistant species) due to limited penetration capacity of conventional cream and liposomes (Aljohani et al., 2024). Therefore, it was imperative to increased access of the drug to the target site of dermal region using OKEL1 and its gel formulation to eradicate these fungal strains. Greater value of %DD suggested maximized drug availability to the dermal area after topical application. Moreover, cationic vesicle could be promising to interplay with negatively charged membrane of fungal hyphae to produce detrimental effect like antibacterial activities (Lu et al., 2022). The existing conventional cream and reported formulation could not achieve the reported permeation profile to execute therapeutic benefit at low cost and high patient compliance. The achieved drug deposition served as deport for slow and sustained access of the drug to the dermal region to cause detrimental effects against fungal hyphae and spores due to added properties in the OKEL1 and its gel.

5. Conclusions

Ketoconazole is a gold standard antifungal agent to treat topical infections. However, deep seated infection is challenging task to treat due to physiological barrier SC and inability of liposomes access to the deeper region. Clinically, available cream, gels, lotions, and shampoos are ineffective to control deeply seated dermal fungal infection due to poor ketoconazole solubility and lack of permeation enhancer. Therefore, the present study addressed the impact of composition of cationic elastic liposomes, permeation insights into skin, and the critical formulation attributes identified in QbD. The composition was optimized using optimal custom design and the design identified the significant impact of components on vesicle size, zeta potential, size distribution, and %EE. The predicted and the actual experimental values of the optimized formulations characteristics were closely related as evidence with the statistical modelling. It was imperative to negate the compatibility of components in the formulation using FTIR tool. In vitro drug release data showed limited release of the drug from suspension due to poor aqueous solubility whereas OKEL1 and corresponding gel exhibited facilitated drug release as compared to liposomes and the drug suspension. The drug release from the gel matrix was slowed down due to viscosity and mitigated diffusion of the drug from lipid bilayer acting as dual drug release limiting barriers. The study was further explored for permeation profile and %DD in rat model. The results showed that %DD was maximized using gel and OKEL1 due to multiple factors working in tandem (composition, formulation characteristics, and gel properties). The proposed cationic elastic liposomes containing SA could be promising over liposomes and nanoemulsions to treat deeply seated fungal strains (clinically resistant and non-resistant variant). Further investigations need to be explored for long term stability at varied temperatures and permeation profile using Human cadaver skin. These studies are still going on by our research team.

Funding

Authors are thankful to the Researchers Supporting Project number (RSPD2024R524), King Saud University, Riyadh, Saudi Arabia, for supporting this work.

CRediT authorship contribution statement

Afzal Hussain: Writing – review & editing, Writing – original draft, Validation, Supervision, Investigation, Conceptualization. **Mohammad A. Altamimi:** Validation, Software, Conceptualization. **Yaser Saleh Alneef:** Methodology, Investigation, Data curation.

Declaration of competing interest

Authors report no conflict of interest.

Data availability

Data will be made available on request.

Acknowledgement

The authors extend their appreciation to the Researchers Supporting Project number (RSPD2024R524), King Saud University, Riyadh, Saudi Arabia, for funding this work.

References

Abbott, S., 2010. Chemical Compatibility of Poly(Lactic Acid): A Practical Framework Using Hansen Solubility Parameters., Chapter 1. John Wiley & Sons, Inc, pp. 83–95.
Aljohani, Alhanouf A., Maryam, A. Alanazi, Lujain, A. Munahhi, Jawaher, D. Hamroon, Mortagi, Y., Qushawy, M., Ghareb, M. Soliman, 2024. Binary ethosomes for the enhanced topical delivery and antifungal efficacy of ketoconazole. OpenNano 11, 100145.
Ba-Abbad, M.M., Kadhum, A.A.H., Mohamad, A.B., Takriff, M.S., Sopian, K., 2013. Optimization of process parameters using D-optimal design for synthesis of ZnO nanoparticles via sol–gel technique. J. Ind. Eng. Chem. 19 (1), 99–105.
Basu, N., Chakraborty, A., Ghosh, R., 2018. Carbohydrate derived organogelators and the corresponding functional gels developed in recent time. Gels 4 (2), 52. https://doi.org/10.3390/gels4020052.
Blume, G., Cevc, G., 1990. Liposomes for the sustained drug release in vivo. Biochim. Biophys. Acta 1029 (1), 91–97.
Cheng, S., Lou, Z., Zhang, L., Guo, H., Wang, Z., Guo, C., Fukuda, K., Ma, S., Wang, G., Someya, T., Cheng, H.-M., Xu, X., 2023. Ultrathin Hydrogel Films toward Breathable Skin-Integrated Electronics. Adv. Mater. 35 (1), 1–15.
Dar, M.J., Khalid, S., Varikuti, S., Satoskar, A.R., Khan, G.M., 2020. Nano-elastic liposomes as multidrug carrier of sodium stibogluconate and ketoconazole: a potential new approach for the topical treatment of cutaneous leishmaniasis. Eur. J. Pharm. Sci. 105256 https://doi.org/10.1016/j.ejps.2020.105256.
De Aguiar, P.F., Bourguignon, B., Khots, M.S., Massart, D.L., Phan-Than-Luu, R., 1995. D-optimal designs. Chemom. Intell. Lab. Syst. 30 (2), 199–210.
Faria, M.J., Machado, R., Ribeiro, A., Gonçalves, H., Real Oliveira, M.E.C.D., Viseu, T., das Neves, J., Lúcio, M., 2019. Rational development of liposomal hydrogels: a strategy for topical vaginal antiretroviral drug delivery in the context of HIV prevention. Pharmaceutics 11, 485. https://doi.org/10.3390/pharmaceutics11090485.
Franzé, S., Donadoni, G., Podestà, A., Procacci, P., Orioli, M., Carini, M., Minghetti, P., Cilurzo, F., 2017. Tuning the extent and depth of penetration of flexible liposomes in human skin. Mol. Pharm. 4 (6), 1998–2009.
Gusai, T., Dhavalkumar, M., Soniwala, M., Dudhat, K., Vasoya, J., Chavda, J., 2020. Formulation and optimization of microsponge-loaded emulgel to improve the transdermal application of acyclovir—a DOE based approach. Drug Deliv. Transl. Res. 11 (5), 2009–2029.
Ha, N.G., Kim, S.L., Lee, S.H., Lee, W.J., 2023. A novel hydrogel-based moisturizing cream composed of hyaluronic acid for patients with xerosis: an intra individual comparative analysis. Skin Res. Technol. 29 (11), e13499 https://doi.org/10.1111/srt.13499.
Hansen, C.M., 2007. Hansen Solubility Parameters: A User's Handbook, 2nd edition. CRC Press, pp. 1–544.
Hussain, A., Singh, S., Sharma, D., Webster, T.J., Shafaat, K., Faruk, A., 2017. Elastic liposomes as novel carriers: recent advances in drug delivery. Int. J. Nanomedicine 12, 5087–5108.
Hussain, A., Alshehri, S., Ramzan, M., Afzal, O., Altamimi, A.S.A., Alossaimi, M.A., 2021. Biocompatible solvent selection based on thermodynamic and computational solubility models, in-silico GastroPlus prediction, and cellular studies of ketoconazole for subcutaneous delivery. J. Drug Deliv. Sci. Technol. 65, 102699 https://doi.org/10.1016/j.jddst.2021.102699.
Hussain, A., Altamimi, M.A., Afzal, O., Altamimi, A.S.A., Ali, A., Ali, A., Martinez, F., Siddique, M.U.M., Acree Jr., W.E., Jouyban, A., 2022. Preferential solvation study of

the synthesized aldose reductase inhibitor (SE415) in the {PEG 400 (1) + Water (2)} cosolvent mixture and GastroPlus-based prediction. ACS Omega 7 (1), 1197–1210.
Kircik, L.H., 2012. Transepidermal water loss (TEWL) and corneometry with hydrogel vehicle in the treatment of atopic dermatitis: a randomized, investigator-blind pilot study. J. Drugs Dermatol. 11 (2), 180–184.
Kumar, P., Singh, S.K., Handa, V., Kathuria, H., 2018. Oleic acid nanovesicles of minoxidil for enhanced follicular delivery. Medicines 5, 103. https://doi.org/10.3390/medicines5030103.
Lin, H.-C., Ko, B.-T., Wu, T.-M., 2019. Thermal and mechanical properties of CO_2-based biodegradable poly(cyclohexene carbonate)/organically modified layered zinc Phenylphosphonate Nanocomposites. J. Polym. Environ. 27, 1065–1070. https://doi.org/10.1007/s10924-019-01414-1.
Lu, P., Zhang, X., Li, F., Xu, K.-F., Li, Y.-H., Liu, X., Yang, J., Zhu, B., Wu, F.-G., 2022. Cationic liposomes with different lipid ratios: antibacterial activity, antibacterial mechanism, and cytotoxicity evaluations. Pharmaceuticals 15, 1556. https://doi.org/10.3390/ph15121556.
Nakamura, D., Hirano, M., Ohta, R., 2017. Nontoxic organic solvents identified using an a priori approach with Hansen solubility parameters. Chem. Commun. 53, 4096. https://doi.org/10.1039/c7cc01434a.
Patel, M.R., Rashmin, B.P., Parikh, J.R., Bhatt, K.K., Solanki, A.B., 2010. Investigating the effect of vehicle on in vitro skin permeation of ketoconazole applied in O/W microemulsions. Acta Pharmaceut. Sci. 52, 65–77.
Prasanthi, D., Lakshmi, P., 2012. Development of ethosomes with taguchi robust design-based studies for transdermal delivery of alfuzosin hydrochloride. Int. Curr. Pharmaceut. J. 1 (11), 370–375.
Ramzan, M., Kaur, G., Trehan, S., Agrewal, J.N., Michniak-Kohn, B.B., Hussain, A., Mahdi, W.A., Gulati, J.S., Kaur, I.P., 2021. Ketoconazole lipidic nanoparticles for improved efficacy, enhanced topical penetration, cellular uptake (L929 and J774A.1), and safety assessment: in vitro and in vivo studies. J. Drug Deliv. Sci. Technol. 65, 102743 https://doi.org/10.1016/j.jddst.2021.102743.
Schlich, M., Musazzi, U.M., Campani, V., Biondi, M., Franzé, S., Lai, F., De Rosa, G., Sinico, C., Cilurzo, F., 2022. Design and development of topical liposomal formulations in a regulatory perspective. Drug Deliv. Transl. Res. 12 (8), 1811–1828. https://doi.org/10.1007/s13346-021-01089-z.
Semalty, A., Tanwar, Y.S., 2013. Nimesulide-phosphatidylcholine complex for improvement of solubility and dissolution. Am. J. Drug Disc. Develop. 3, 225–234.
Shahid, M., Hussain, A., Khan, A.A., Ramzan, M., Alaofi, A.A., Alanazi, A.M., Alanazi, M. M., Rauf, M.A., 2022. Ketoconazole-loaded cationic nanoemulsion: in vitro–ex vivo–in vivo evaluations to control cutaneous fungal infections. ACS Omega 7 (23), 20267–20279.
Slavkova, M., Tzankov, B., Popova, T., Voycheva, C., 2023. Gel formulations for topical treatment of skin cancer: a review. Gels 9, 352. https://doi.org/10.3390/gels9050352.
Smith, E.B., Henry, J.C., 1984. Ketoconazole: an orally effective antifungal agent. Mechanism of action, pharmacology, clinical efficacy and adverse effects. Pharmacotherapy 4 (4), 199–204.
Sodeifian, G., Sajadian, S.A., Razmimanesh, F., Hazaveie, S.M., 2021. Solubility of Ketoconazole (antifungal drug) in SC-CO_2 for binary and ternary systems: measurements and empirical correlations. Sci. Rep. 11 (1), 7546. https://doi.org/10.1038/s41598-021-87243-6.
Tahara, K., Kobayashi, M., Yoshida, S., Onodera, R., Inoue, N., Takeuchi, H., 2018. Effects of cationic liposomes with stearylamine against virus infection. Int. J. Pharm. 543 (1–2), 311–317.
Vassoudevane, J., Mariebernard, M., Rajendran, V., 2023. Stearylamine liposome as an anti-parasitic agent. Drugs Drug Candidat. 2, 95–108.
Yoshihara, E., Nakae, T., 1986. Cytolytic activity of liposomes containing stearylamine. Biochim. Biophys. Acta (BBA)-Biomembr. 854, 93–101.
Zen, N.I., Abd, Gani, S.S., Shamsudin, R., Masoumi, H.R., 2015. The use of D-optimal mixture design in optimizing development of okara tablet formulation as a dietary supplement. Sci. World J. 2015, 684319 https://doi.org/10.1155/2015/684319.